Analysis of Self-Cooling with Infiltrated Porous Tungsten Composites

F. B. GESSNER*
American-Standard, New Brunswick, N. J.

J. D. SEADER,§ R. J. INGRAM,‡ AND T. A. COULTAS§
North American Aviation, Canoga Park, Calif.

With the advent of solid rocket engines utilizing high-energy aluminized propellants, the need for a noneroding nozzle-throat insert material has become acute. The wall temperatures attained at the throat are above even the maximum practical operating temperature of tungsten. However, by infiltrating a porous tungsten insert with a second material, which is subject to gasification by boiling, sublimation, or decomposition, it is possible to reduce the wall temperature to a tolerable value. This paper presents an analysis of the behavior of this so-called "self-cooling" process with infiltrated porous tungsten composites. A one-dimensional, finite thickness, flat plate model is specified. As gasification of the infiltrant proceeds, the gaseous/liquid or solid infiltrant interface recedes from the surface. The transient partial differential equations describing the model consist of the continuity, momentum, and energy relations. The effect of transpiration is included. The equations are solved by a numerical finite-difference solution that was programed for the IBM 7094. Typical results of the computer program are presented for a number of organic and inorganic infiltrants at typical high-pressure solid rocket nozzle-throat conditions to illustrate the effects of certain variables such as porosity and permeability of the porous tungsten.

Nomenclature

A = intercept of a vapor pressure/temperature curve
B = slope of a vapor pressure/temperature curve
C = specific heat
C_c = infiltrant specific heat
$(C_c)_g$ = infiltrant vapor specific heat
C_m = matrix material specific heat
C_g = hot-gas specific heat
$(G_c)_g$ = superficial mass velocity of infiltrant vapor through porous structure
G_g = hot-gas mass velocity
g_c = universal constant
h_0 = convective heat-transfer coefficient with no transpiration
h = convective heat-transfer coefficient with transpiration
k = thermal conductivity
k_c = infiltrant thermal conductivity
k_m = matrix material thermal conductivity
L = composite thickness
M = molecular weight
P_g = hot-gas pressure
P_v = pressure at interface
P = interconnected porosity
R = gas constant
$(Re)_D$ = hot-gas Reynolds number based on throat diameter
$(St)_0$ = Stanton number with no transpiration
T = temperature
T_g = hot-gas recovery temperature
T_v = interface temperature
$(T_v)_1$ = temperature at which interface recession begins
T_0 = initial composite temperature
T_s = constant surface temperature
x = distance into composite
Δx = distance increment
α = viscous flow coefficient
β = inertial flow coefficient
δ = porous structure thickness
θ = time
θ_1 = time at which interface recession begins
θ_{max} = time at which interface recession ends
$\Delta\theta$ = time increment
λ_v = infiltrant heat of vaporization at interface temperature
$(\mu_c)_g$ = infiltrant vapor viscosity
ρ_c = infiltrant density
ρ_m = matrix material density
ρ = density

Subscripts

1, 2, 3 = element number
b = last element
c = infiltrant
m = matrix material
r = element
v = element containing interface

Superscripts

$()'$ = quantities after one time increment

Presented as Preprint 64-104 at the AIAA Solid Propellant Rocket Conference, Palo Alto, Calif., January 29–31, 1964; revision received June 24, 1964. This study was conducted by the Combustion, Heat Transfer and Fluid Dynamics Group of the Research Center at Santa Susana, Calif. and was supported by the Metals and Ceramics Laboratory, Materials Central, U. S. Air Force, under Contract No. AF33(657)-9166.

* Research Scientist, Fluid Mechanics Section.

† Principal Scientist, Heat Transfer and Fluid Dynamics Unit, Rocketdyne Division. Member AIAA.

‡ Engineering Associate, Heat Transfer and Fluid Dynamics Unit, Rocketdyne Division.

§ Group Scientist, Combustion, Heat Transfer and Fluid Dynamics Group, Rocketdyne Division. Associate Fellow Member AIAA.

Introduction

THE development of high-energy aluminized propellants with flame temperatures in excess of 6000°F has created the need for a new noneroding nozzle-throat insert material for solid rocket motors. The nozzle wall temperatures attained with these high-energy propellants during a firing period of reasonable duration exceed even the maximum practical operating temperature of uncooled tungsten. However, by infiltrating a porous tungsten insert with a second material that is subject to gasification by boiling, sublimation, or decomposition, it is possible to reduce the wall temperature to a tolerable value. This concept has been termed "self-cooling" by Schwarzkopf and Weisert.[1]

Initial development of the infiltrated porous tungsten self-cooling concept was carried out by Maloof[2] and Davies

and Smith[3] with copper and lithium hydride infiltrants, respectively. More recently Robinson, McAlexander, Ramsdell, and Wolfson[4] conducted nozzle firing tests with both infiltrated porous tungsten (copper and brass infiltrants) and tungsten metal-oxide (BeO and Al_2O_3) compacts. They also carried out laboratory plasma arc tests. Baranow and Hiltz[5] presented a general discussion of the self-cooling concept and compared possible infiltrants on the basis of a steady-state vaporization of infiltrant. Most recently, Schwarzkopf and Weisert[1] developed fabrication techniques to produce tungsten composites of closely controlled properties, and conducted a large number of micromotor firing tests with a number of organic and inorganic infiltrants.

Despite the rapid growth of interest in the self-cooling concept and the relatively large number of firing tests which have been conducted, no adequate theoretical model and accompanying analysis of the concept have been presented. Therefore, in order to guide the selection of appropriate infiltrants and porous structures or compacts, aid the interpretation of experimental results, and give insight into the effect of the various composite variables such as porosity and permeability, a comprehensive theoretical analysis was developed and programed[6] for the IBM 7094 digital computer. Case studies were run for a number of infiltrants in a porous tungsten matrix. A summary of the important details of the analysis and its application are presented.

Theoretical Model

Consider the flow of hot gas through a rocket nozzle having a throat insert consisting of a porous refractory matrix, which is filled with an organic or inorganic infiltrant. If the thickness of the insert is small compared to the nozzle-throat radius, the insert can be considered to be an infinite plate of finite thickness. The plate is considered to be a tungsten-infiltrant composite of constant porosity with a single infiltrant that vaporizes below the melting point of the refractory matrix. The heating process can be described as follows. The plate is initially at a uniform temperature. At some later instant, a sudden change in environmental temperature occurs because of hot-gas flow. Heating of the surface in contact with the hot gas occurs. (The back surface is considered to be thermally insulated.) When the infiltrant boiling point is reached, a liquid/vapor interface begins to recede and infiltrant vapor starts to flow through the porous matrix structure. A schematic diagram of the model after heating has begun and the liquid/vapor interface has formed is given in Fig. 1. Recession of the liquid/vapor interface continues until heating is ended or until the infiltrant is exhausted.

To simplify the analysis, the following conditions are prescribed:

1) one-dimensional, unsteady-state heat transfer,
2) temperature-constant thermophysical properties,
3) equal matrix and infiltrant vapor temperatures at a given depth in the porous structure,
4) heat of fusion of infiltrant combined with heat of vaporization,
5) heat conducted through infiltrant in gaseous phase negligible compared to heat conducted through porous matrix,

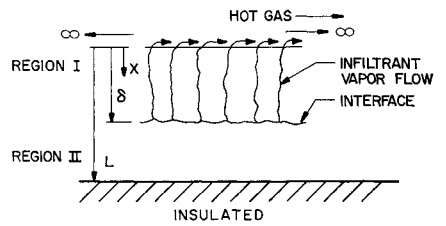

Fig. 1 Model after the liquid/vapor interface has formed.

6) radiation between hot gas and heated surface negligible compared to convective heating,
7) no diffusion or chemical reactions between infiltrant vapor and hot gas,
8) radiation within porous structure neglected.

Theoretical Equations

After heating has begun but before vaporization of the infiltrant occurs, a heat balance on any internal volume element can be written as

$$[k_m(1 - P) + k_cP]\frac{\partial^2 T}{\partial x^2} = [\rho_m C_m(1 - P) + \rho_c C_c P]\frac{\partial T}{\partial \theta} \tag{1}$$

where

$$T = T(x, \theta)$$

The corresponding initial condition and boundary conditions are as follows

$$T(x, 0) = T_0 \tag{2}$$

$$-[k_m(1 - P) + k_cP]\left(\frac{\partial T}{\partial x}\right)_{x=0} = h_0(T_g - T)_{x=0} \qquad (0 < \theta < \theta_1) \tag{3}$$

$$(\partial T/\partial x)_{x=L} = 0 \qquad (0 < \theta < \theta_1) \tag{4}$$

After vaporization occurs and a liquid/vapor interface has formed, two regions exist for which heat balances must be written, as shown in Fig. 1. The first region is between the heated surface and the interface, and the second is between the interface and the insulated surface. The heat balances and corresponding initial and boundary conditions can be written as follows.

Region 1: between heated surface and liquid/vapor interface

$$0 \leq x \leq \delta$$

$$k_m(1 - P)\frac{\partial^2 T}{\partial x^2} + (C_c)_g(G_c)_g\frac{\partial T}{\partial x} = \rho_m C_m(1 - P)\frac{\partial T}{\partial \theta} \tag{5}$$

with

$$-k_m(1 - P)\left(\frac{\partial T}{\partial x}\right)_{x=0} = h(T_g - T) \qquad (\theta_1 \leq \theta \leq \theta_{\max}) \tag{6}$$

$$-k_m(1 - P)\left(\frac{\partial T}{\partial x}\right)_{\delta^-} = (G_c)_g\lambda_v - [k_m(1 - P) + k_cP]\left(\frac{\partial T}{\partial x}\right)_{\delta^+} \qquad (\theta_1 \leq \theta \leq \theta_{\max}) \tag{7}$$

Region 2: between liquid/vapor interface and insulated surface

$$\delta < x \leq L$$

$$[k_m(1 - P) + k_cP]\frac{\partial^2 T}{\partial x^2} = [\rho_m C_m(1 - P) + \rho_c C_c P]\frac{\partial T}{\partial \theta} \tag{8}$$

with Eq. (7) applicable at the interface and with

$$(\partial T/\partial x)_{x=L} = 0 \qquad (\theta_1 \leq \theta \leq \theta_{\max}) \tag{9}$$

In addition to the boundary condition at the liquid/vapor interface given by Eq. (7), a continuity equation at the interface also can be written stating that the infiltrant vapor mass flow rate is proportional to the interface recession rate. That is,

$$(G_c)_g = \rho_c P(\partial\delta/\partial\theta) \qquad (\theta_1 \leq \theta \leq \theta_{\max}) \tag{10}$$

When heating has begun but before vaporization of the infiltrant occurs ($0 < \theta < \theta_1$), the temperature distributions can be determined readily in closed form from Eq. (1) by the customary separation-of-variables technique. Typical solutions are given by Heisler.[7] At the instant the infiltrant vaporizes, however, a set of two partial differential equations [Eqs. (5) and (8)] must be solved which are coupled by the interface condition [Eq. (7)]. A closed-form solution to these equations was obtained by Grosh[8] for quite different boundary conditions than given previously. He considered a semi-infinite slab ($L = \infty$) and a constant surface temperature boundary condition [$T(0, \theta) = T_s$] instead of the variable heat flux condition given by Eq. (6). A closed-form solution for the complete set of equations and boundary conditions presented previously did not appear possible. Therefore, a finite difference numerical approach for solving the set of equations was developed. Such an approach often is used for heat conduction problems as discussed by Dusinberre.[9] Because little additional effort was required, the transpiration effect of the infiltrant vapor flow on the convective heat-transfer coefficient was included, as well as the variation of heat of vaporization with interface temperature. The pressure drop through the depleted porous structure due to viscous and inertial effects caused by the infiltrant vapor flow also was taken into account.

Numerical Finite-Difference Solution

Based upon the foregoing model and theory, a one-dimensional numerical solution was programed for the IBM 7094 in order to determine liquid/vapor interface recession rates and temperature distributions. Except for the latent heat, physical properties were assumed to be independent of temperature. A diagram of the model for numerical solution is shown in Fig. 2. The equations used were heat balance relations in finite difference form for elements 1 through b of size Δx. These equations were solved for the temperature T' after a time increment $\Delta\theta$. An explicit, forward finite-difference technique was utilized. For the *initial heating period* the finite difference equations are as follows: Element 1:

$$T_1' = T_1 + \frac{2\Delta\theta}{[\rho_m C_m(1-P) + \rho_c C_c P]\Delta x} \times \left\{h_0(T_g - T_1) - [k_m(1-P) + k_c P]\frac{(T_1 - T_2)}{\Delta x}\right\} \quad (11)$$

Elements 2 through $b - 1$:

$$T_r' = T_r + \frac{\Delta\theta[k_m(1-P) + k_c P]}{[\rho_m C_m(1-P) + \rho_c C_c P](\Delta x)^2} \times (T_{r-1} + T_{r+1} - 2T_r) \quad (12)$$

where $r = 2, 3, \ldots, b - 1$.

Element b:

$$T_b' = T_b + \frac{2\Delta\theta[k_m(1-P) + k_c P]}{[\rho_m C_m(1-P) + \rho_c C_c P](\Delta x)^2}(T_{b-1} - T_b) \quad (13)$$

As would be expected, the solution to Eqs. (11–13) for $\theta < \theta_1$ was in excellent agreement with the closed-form solution as given by Heisler.[7]

For the *interface recession period*, the finite difference equations are as follows.

Interface within Element 1

Element 1:

$$T_1' = B/(A - \log_{10}P_v) \qquad \text{(vapor-pressure relation)} \quad (14)$$

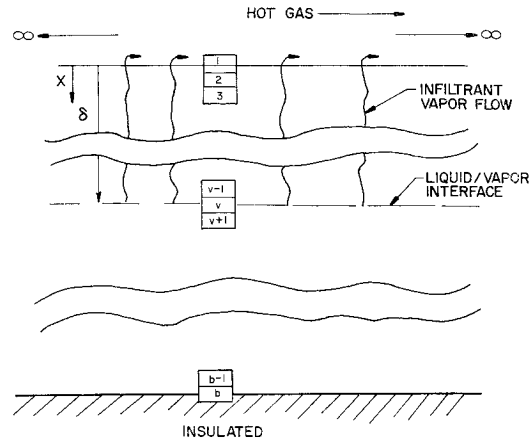

Fig. 2 Elemental model for numerical solution.

Elements 2 through $b - 1$: Eq. (12)
Element b: Eq. (13)
Mass flow rate of infiltrant vapor:

$$(G_c)_g = \frac{1}{\lambda_v}\left[h(T_g - T_1) - \frac{k_m(1-P) + k_c P}{\Delta x}(T_1 - T_2)\right] \quad (15)$$

Liquid/Vapor Interface within Elements 2 through $b - 1$

Element 1:

$$T_1' = T_1 + \frac{2\Delta\theta}{\rho_m C_m(1-P)\Delta x}\left[h(T_g - T_1) - \frac{k_m(1-P)}{\Delta x}(T_1 - T_2) - (C_c)_g(G_c)_g\frac{(T_1 - T_2)}{2}\right] \quad (16)$$

Elements 2 through $(v - 1)$:

$$T_r' = T_r + \frac{\Delta\theta}{\rho_m C_m(1-P)\Delta x}\left[\frac{k_m(1-P)}{\Delta x} \times (T_{r-1} + T_{r+1} - 2T_r) - (C_c)_g(G_c)_g\frac{(T_{r-1} - T_{r+1})}{2}\right] \quad (17)$$

Element v:

$$T_v' = B/(A - \log_{10}P_v) \quad (18)$$

Elements $(v + 1)$ through $(b - 1)$: Eq. (12)
Element b: Eq. (13)
Mass flow rate of infiltrant vapor:

$$(G_c)_g = \frac{1}{\lambda_v + (C_c)_g\dfrac{(T_{v-1} - T_v)}{2}}\left[\frac{k_m(1-P)}{\Delta x}(T_{v-1} - T_v) - \frac{k_m(1-P) + k_c P}{\Delta x}(T_v - T_{v+1})\right] \quad (19)$$

Interface within Element b

Element 1: Eq. (16)
Elements 2 through $(b - 1)$: Eq. (17)
Element b: Eq. (18)
Mass flow rate of infiltrant vapor:

$$(G_c)_g = \frac{k_m(1-P)}{\lambda_v + (C_c)_g\dfrac{(T_{v-1} - T_v)}{2}}\left[\frac{T_{v-1} - T_v}{\Delta x}\right] \quad (20)$$

Interface recession is determined with respect to time from the following equation:

$$\delta' = \delta + (G_c)_g\Delta\theta/(\rho_c P) \quad (21)$$

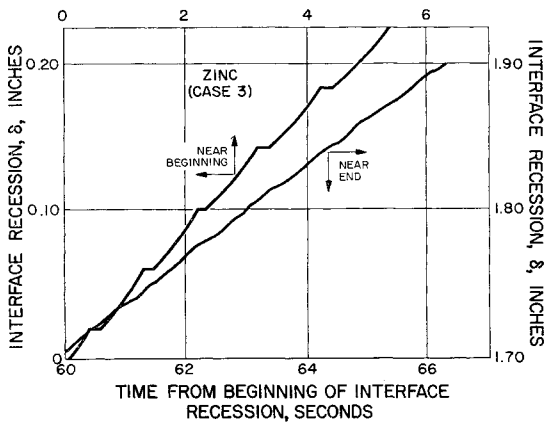

Fig. 3 Typical interface recession curves.

The solution of Eqs. (11–21) depends upon the interrelation of the dependence of heat of vaporization on interface temperature and the effects of pressure and temperature on the infiltrant vapor mass flow rate which, in turn, affect the convective heat-transfer coefficient by the transpiration effect. Appropriate relations were used for the transpiration effect, latent heat, infiltrant pressure drop, and infiltrant vapor pressure as follows.

The reduction of the convective heat-transfer coefficient from the hot gas to the nozzle insert surface because of infiltrant vapor flow into the hot-gas boundary layer was determined from the following expression developed by Bartle and Leadon,[10] based on the work of Friedman[11]:

$$h = h_0 \xi/(e^{\xi} - 1) \tag{22}$$

where

$$\xi = r(C_c)_g(G_c)_g/C_gG_g(\mathrm{St})_0$$

and

$$r = 2.11\ (Re)_D{}^{-0.1} \tag{23}$$

The effect of temperature on the latent heat was computed from Watson's equation.[12] The infiltrant vapor pressure was calculated from either Eq. (14) or (18). The pressure drop for the flow of infiltrant vapor through the porous matrix was determined from the following equation of Green and Duwez[13] which includes both viscous and inertial effects:

$$P_v = \left\{P_g{}^2 + \delta\left[2\frac{\alpha R}{g_c M}(\mu_c)_g(G_c)_g + 2\frac{\beta R}{g_c M}(G_c)_g{}^2\right]\sum_{r=1}^{v}\frac{T_r}{v}\right\}^{1/2} \tag{24}$$

The viscous and inertial flow coefficients α and β are related to the matrix permeability. The average infiltrant vapor temperature over the recession distance was used to obtain the infiltrant vapor viscosity as estimated from the relations presented by Gambill.[14]

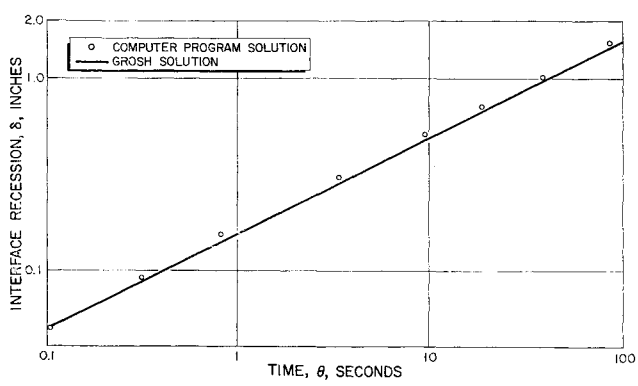

Fig. 4 Comparison of computed interface recession distance with Grosh solution: zinc, P = 0.3.

The procedure for calculating temperature distributions, pressures, and temperatures at the interface, interface recession rates, infiltrant vapor flow rates, and convective heat-transfer coefficients in the computer program was as follows: The distance and time increments, Δx and $\Delta\theta$, respectively, were first chosen in accordance with appropriate stability criteria as discussed by Dusinberre.[9] From the onset of heating to the time when the surface temperature reached the infiltrant boiling temperature at the local pressure, Eqs. (11–13) were used to calculate temperature distributions. At the time interface recession began θ_1, the temperature distribution was therefore known. The latent heat of vaporization λ_v was then calculated from Watson's equation using the surface temperature calculated at time θ_1. This value of λ_v, together with a specified value for the heat-transfer coefficient with no transpiration h_0 and the temperatures of elements 1 and 2 at time θ_1, was used to calculate an initial value of infiltrant vapor mass velocity $(G_c)_g$ from Eq. (15). This value of $(G_c)_g$ was then used to calculate a new value of h from Eq. (22) and an initial value of the interface recession δ over the next time increment from Eq. (21). Subsequently, the interface recession distance was examined in order to determine which element the interface was within. Temperature distributions were then calculated at the new time from the proper set of finite difference equations using the temperatures calculated at time θ_1. After the temperature distribution had been determined, the infiltrant vapor viscosity was calculated from the Gambill relations, and the interface pressure was determined from Eq. (24). At this point the surface temperature was examined in order to determine whether it had reached or exceeded the melting temperature of the tungsten matrix. If this was the case, the calculations were terminated. If not, the computer moved into the next time increment and repeated the calculations until one of the following conditions was reached: 1) the surface temperature equaled the melting point of tungsten (6100°F), 2) all of the infiltrant was vaporized, 3) a prohibitive vapor pressure drop occurred, or 4) the sum of time increments totaled the prescribed maximum heating time (200 sec).

Throughout the calculations, if the interface remained within the same element over any time increment, the temperature of that element remained the same. During this time, the remaining elements were allowed to rise in temperature with time according to the heat balance equations. This caused the infiltrant vapor mass velocity to oscillate and also caused the interface recession δ to proceed in a somewhat stepped-fashion which gradually damped-out, as shown in Fig. 3 for the case of a zinc infiltrant. Despite these effects on δ and $(G_c)_g$, over-all heat balances were maintained, and average values over a time period corresponding to the movement of the interface through an element Δx were found to be correct within about 5%.

Table 1 Values of test conditions and material properties for comparison to Grosh solution

Condition		Value
T_s, °F		6020
T_0, °F		0
P, %		30
T_v, °F		2584
λ_v, Btu/lb		615
$(C_c)_g$, Btu/lb-°F		0.076
Property	Tungsten	Zinc
k, Btu/hr-ft-°F	60.0	60.0
ρ, lb/cu ft	1210	445
C, Btu/lb-°F	0.050[a]	0.13

[a] This value is different from the value given in Table 2 (0.0385) because different conditions are imposed on the temperature variation of the tungsten matrix for the two cases.

Table 2 Infiltrant properties and specific parameters for case studies

	Matrix	Infiltrant				
Property of parameter	Tungsten	Silver, case 1	Silver, case 2	Silver, case 14	Zinc, case 3	Teflon, case 7
$(C_c)_g$, Btu/lb-°F			0.046		0.076	0.2
C, Btu/lb-°F	0.0385		0.0744		0.130	0.3
ρ, lb/ft³	1204		654		445	137.3
k, Btu/hr-ft-°F	60		200		54	0.14
$(T_v)_1$, °F at 226 psia			5243		2313	1400[a]
A, lb$_f$/ft²			8.79		8.39	
B, lb$_f$-°F/ft²			24,400		10,753	
α, ft^{-2} × 10^{-11}		3.71	371.6	3.71	3.71	3.71
β, ft^{-1} × 10^{-7}		1.525	30,480	1.525	1.525	1.525
Porosity		0.2	0.2	0.8	0.2	0.2

[a] Constant at all pressures.

Comparison with Grosh Solution

To check the accuracy of the one-dimensional finite difference computer program solution, a comparison was made to the restricted theoretical, closed-form solution of Grosh.[8] As has been mentioned, this solution assumes a constant surface temperature and an infinitely thick insert; also, it neglects infiltrant vapor pressure drop through the depleted matrix. The results of the comparison for a typical case of porous tungsten infiltrated with zinc are shown in Fig. 4, in which the interface recession distance is plotted against time, based on the values in Table 1. As is shown, excellent agreement was obtained. Similar excellent agreement was obtained between the calculated temperature distributions. The comparison thus served to indicate the accuracy of the numerical solution.

Case Studies

Relative effectiveness of a number of different infiltrants including silver, zinc, magnesium, lithium, Teflon, tin, ammonium chloride, lithium chloride, and several hypothetical materials are included in Ref. 6. Important results for case studies involving silver, zinc, and Teflon are presented here.

The general conditions selected for all cases were as follows, based on throat conditions for a typical solid rocket engine with a 2-in.-thick insert:

T_g = 6200°F
$(Re)_D$ = 190,000
G_g = 1,233,000 lb/hr-ft²
C_g = 0.446 Btu/lb-°F
P_g = 226 psia
$(St)_0$ = 0.00237
h_0 = 1303 Btu/hr-ft²-°F
T_0 = 70°F

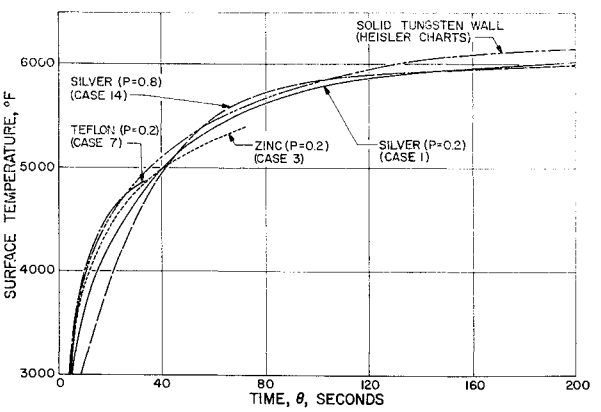

Fig. 5 Comparison of heated surface temperatures for various infiltrants in a constant porosity matrix.

Tungsten and infiltrant properties are listed in Table 2. Cases 1, 3, and 7 are base cases to compare silver, zinc, and Teflon. Case 2 is a low permeability silver composite and case 14 is a high porosity silver composite. For all cases, the distance and time increments used in the computer program were 0.04 in. and 0.005 sec, respectively.

The resulting variations of surface temperature and interface recession with time as determined from the computer program are given in Figs. 5 and 6, respectively. The surface temperature rise of pure tungsten, as computed from the Heisler charts, is also included for comparison in Fig. 5.

Silver (Case 1)

The beginning of recession θ_1 does not occur until 47.9 sec for silver because of its high boiling point and, to a lesser extent, the high thermal diffusivity of the composite. During this period, the heated surface of the composite slab is cooler than a slab of solid tungsten. However, the two curves tend to converge as the boiling point of silver (5243°F) is approached. The calculations showed that the reduction of the convective heat-transfer coefficient h is small (h/h_0 = 0.99) at 90 sec (well into recession), so that the contribution of transpiration cooling to the retardation of the hot-surface temperature rise is negligible. A renewed inhibition of the surface temperature after recession begins is evidenced by the trend of the silver curve away from the tungsten curve toward lower rates of temperature rise after about 80 sec. This beneficial result occurs because of the high volumetric latent heat of silver, which results in slow interface recession.

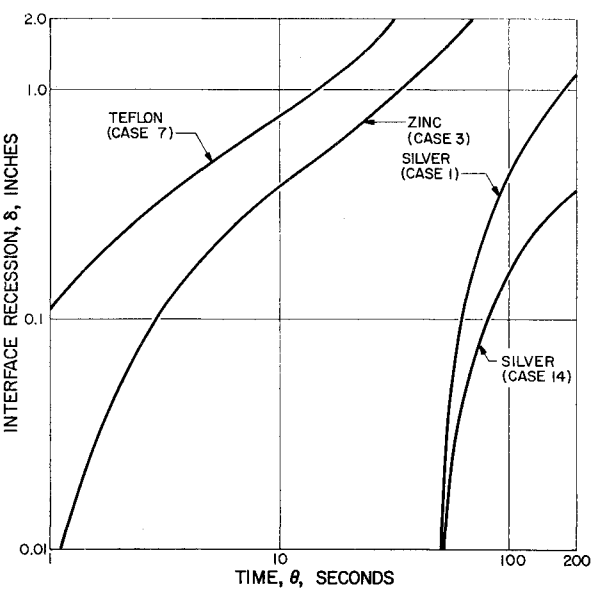

Fig. 6 Interface recession for various infiltrants in a constant porosity matrix.

The high boiling point of silver, however, limits the degree of surface temperature reduction that can be obtained.

Zinc (Case 3)

The low boiling point of zinc (2313°F) results in almost immediate interface recession ($\theta_1 = 1.3$ sec). After about 5 sec, a slower rate of surface temperature rise is noted for the zinc composite than for pure tungsten. This divergence increases until the zinc coolant is exhausted at 72 sec. Again the calculations showed that the transpiration effect is very small ($h/h_0 = 0.98$ at 30 sec). The surface temperature inhibition is due primarily to the low boiling point of zinc. The degree of surface temperature reduction is limited by the relatively low volumetric latent heat of zinc which causes a relatively fast interface recession rate. Zinc is markedly superior to silver until the zinc is exhausted.

Teflon (Case 7)

The very low dissociation temperature (1400°F) and low thermal diffusivity of the Teflon composite cause almost immediate recession ($\theta_1 = 0.25$ sec). However, the low temperature of the vapor/solid interface is counteracted by the very rapid interface recession rate, attributable to the low-volumetric latent heat. Teflon showed only a slight increase in the transpiration cooling effect ($h/h_0 = 0.97$). Exhaustion of the infiltrant occurred in only about 30 sec.

Silver (Case 2)

Case 2 was formulated in order to compare the effect of matrix permeability with that for case 1. For case 1, the values of α and β shown in Table 2 correspond to a tungsten powder size of about 50 μ. The resulting calculated infiltrant vapor pressure drop through the porous matrix was never greater than 135 psi during the 200-sec duration. For case 2, a less permeable matrix was assumed, as indicated by the values of α and β shown in Table 2. These values correspond to a powder size of less than 10 μ. For this case, the calculated pressure drop increased rapidly to almost 1000 psi within 4 sec after recession began. The run was terminated because the infiltrant vapor temperature corresponding to the high interface pressure exceeded the assumed hot-gas recovery temperature.

Silver (Case 14)

All of the cases previously discussed were for a matrix porosity of 20%; case 14 is for an 80% porous matrix. Recession for case 14 commences at about the same time as for case 1 (Fig. 6). However, a considerably different surface temperature rise occurs prior to recession. After recession has proceeded for some time, the two surface temperature curves begin to converge (Fig. 5). Thus, a severely reduced cross-sectional area for conduction through the depleted 80% porous matrix is counterbalanced by the slower infiltrant recession rate accompanying the increased volume of available infiltrant. Increased porosity can significantly reduce the composite thickness requirement (Fig. 6).

Conclusions

A detailed theoretical analysis has shown that the well-known transient conduction effects contribute to the pre-recession behavior of composites with high thermal diffusivities. This effect is probably most important with respect to thermal shock. The role of transpiration cooling is very small for the cases considered. The concept of a composite material that retards its own heating rate by sacrifice of an infiltrant phase has been shown to be theoretically sound. It appears that the degree and duration of self-cooling can be controlled to provide superior nozzle materials for the more hostile thermal environments anticipated in rocket engines. An ideal infiltrant should have a low boiling point and a high volumetric latent heat.

Extension of Analysis

A revision to extend the usefulness of the analysis is currently being conducted. A new version of the computer program will allow the matrix porosity to be varied as either an exponential, power series, or step function of distance beneath the heated surface. The improved program will also allow thermal conductivity and specific heat to be temperature-dependent functions. The oscillations in infiltrant vapor mass velocity previously described will be eliminated by allowing a temperature gradient to exist in the element containing the interface. Further extension of the program to handle a three-dimensional rocket nozzle geometry, including both self-cooling and ordinary heat sink materials, is being considered.

References

[1] Schwarzkopf, P. and Weisert, E. D., "Self-cooled rocket nozzles," AIAA Preprint 64-129 (January 29–31, 1964).

[2] Maloof, S. K., "Development of ultra-high temperature tungsten base composites for rocket nozzle applications," ARS Preprint 1573-60 (December 1960).

[3] Davies, G. F. and Smith, W. E., "Development of refractory materials for rocket nozzles and vanes," Clevite Corp. Summary Rept. NOrd 18887 (May 19, 1960).

[4] Robinson, A. T., McAlexander, R. L., Ramsdell, J. D., and Wolfson, M. R., "Transpiration cooling with liquid metals," AIAA J. **1**, 89–95 (1963).

[5] Baranow, S. and Hiltz, R. H., "The performance and application of porous infiltrated tungsten structures as inserts in solid propellant rocket nozzles," ARS Preprint 2413-62 (April 1962).

[6] Gessner, F. B., Ingram, R. J., and Seader, J. D., "Summary report, self-cooled rocket nozzles," Rocketdyne Rept. R-5323, Vol. 2, Rocketdyne Div., Canoga Park, Calif.; also Wright Aeronautical Systems Div. Rept. RTD-TDR-63-4046 (U), Contract AF33(657)-9166, Wright-Patterson Air Force Base, Ohio (March 1964).

[7] Heisler, M. P., "Temperature charts for conduction and constant-temperature heating," Trans. Am. Soc. Mech. Engrs. **69**, 227–236 (1947).

[8] Grosh, R. J., "Transient temperature change in semi-infinite porous solid with phase change and transpiration effects," Wright Air Development Div. TR 60-105 (January 1960).

[9] Dusinberre, G. M., *Heat-Transfer Calculations by Finite Differences* (International Textbook Co., Scranton, Pa., 1961).

[10] Bartle, E. R. and Leadon, B. M., "Experimental evaluation of heat transfer with transpiration cooling in a turbulent boundary layer at $M = 3.2$," J. Aerospace Sci. **27**, 78–80 (1960).

[11] Friedman, J., "A theoretical and experimental investigation of rocket-motor sweat cooling," ARS J. **19**, 147–154 (1949).

[12] Watson, K. M., "Thermodynamics of the liquid state, generalized prediction of properties," Ind. Eng. Chem. **35**, 398–406 (1943).

[13] Green, L. and Duwez, P., "Fluid flow through porous metals," Trans. Am. Soc. Mech. Engrs. **72**, 39–45 (1951).

[14] Gambill, W. R., "Estimate low-pressure gas viscosity," Chem. Eng. **65**, 169–172 (September 22, 1958).